



## Strathprints Institutional Repository

**Kostas, K. V. and Ginnis, A. I. and Politis, C. G. and Kaklis, P. D. (2015) Ship-hull shape optimization with a T-spline based BEM-isogeometric solver. Computer Methods in Applied Mechanics and Engineering, 284. pp. 611-622. ISSN 0045-7825 , <http://dx.doi.org/10.1016/j.cma.2014.10.030>**

This version is available at <http://strathprints.strath.ac.uk/53880/>

**Strathprints** is designed to allow users to access the research output of the University of Strathclyde. Unless otherwise explicitly stated on the manuscript, Copyright © and Moral Rights for the papers on this site are retained by the individual authors and/or other copyright owners. Please check the manuscript for details of any other licences that may have been applied. You may not engage in further distribution of the material for any profitmaking activities or any commercial gain. You may freely distribute both the url (<http://strathprints.strath.ac.uk/>) and the content of this paper for research or private study, educational, or not-for-profit purposes without prior permission or charge.

Any correspondence concerning this service should be sent to Strathprints administrator: [strathprints@strath.ac.uk](mailto:strathprints@strath.ac.uk)

# Ship-Hull Shape Optimization with a T-spline based BEM-Isogeometric Solver

K.V. Kostas<sup>a,\*</sup>, A.I. Ginnis<sup>b</sup>, C.G. Politis<sup>a</sup>, P.D. Kaklis<sup>c</sup>

<sup>a</sup>*Department of Naval Architecture, Technological Educational Institute of Athens*

<sup>b</sup>*School of Naval Architecture & Marine Engineering, National Technical University of Athens*

<sup>c</sup>*Department of Naval Architecture, Ocean and Marine Engineering, University of Strathclyde*

---

## Abstract

In this work, we present a ship-hull optimization process combining a T-spline based parametric ship-hull model and an Isogeometric Analysis (IGA) hydrodynamic solver for the calculation of ship wave resistance. The surface representation of the ship-hull instances comprise one cubic T-spline with extraordinary points, ensuring  $C^2$  continuity everywhere except for the vicinity of extraordinary points where  $G^1$  continuity is achieved. The employed solver for ship wave resistance is based on the Neumann-Kelvin formulation of the problem, where the resulting Boundary Integral Equation is numerically solved using a higher order collocated Boundary Element Method which adopts the IGA concept and the T-spline representation for the ship-hull surface. The hydrodynamic solver along with the ship parametric model are subsequently integrated within an appropriate optimization environment for local and global ship-hull optimizations against the criterion of minimum resistance.

---

## 1. INTRODUCTION

Due to an increasing demand for efficiency and robustness in *Computer Aided Ship Design (CASD)*, the available modeling, analysis and evaluation techniques are being continuously pushed forward so that they can provide measurable improvements for both the design process and the resulting product. Fortunately, the current availability of computing power has allowed the employment of sophisticated *Computational Fluid Dynamic (CFD)* solvers and their coupling with advanced *Geometric Modeling* techniques and *Optimization* strategies, a combination that offers significant aid to meet the demanding requirements of contemporary CASD.

The optimization of a hull-form with respect to its resistance and resulting fuel consumption has always been a major task in ship design. Moreover, as the design of the hull form is a prerequisite for the majority of ship design tasks, it is of great importance to complete this task in the earliest possible time. The present work is focused in developing an appropriate ship-hull hydrodynamic

---

\*Corresponding author: kvkostas@teiath.gr

1  
2  
3  
4  
5  
6  
7 optimization process, combining modern optimization techniques, a fully parametric T-spline ship-  
8 hull model and a BEM hydrodynamic solver. Both the parametric model and hydrodynamic solver  
9 are in-house developed. Note that the hydrodynamic solver adopts the concept of *Isogeometric*  
10 *Analysis (IGA)*, introduced by Hughes et al. [1], which aims to intrinsically integrate CAD with  
11 Analysis by communicating the CAD model of the geometry (ship hull) to the solver without any  
12 approximation, e.g., panelization. Furthermore, Basilevs et al [2] and Scott et al [3] have already  
13 demonstrated the efficient usage of IGA in conjunction with T-splines technology [4, 5]. **Shape**  
14 **optimization, in the context of IGA, has been presented in various works as, e.g., in [6, 7, 8] for**  
15 **the 2D case and in [9] for the 3D case. In these works, the control points are directly used as**  
16 **shape optimization parameters. In our case, due to the shape complexity and restrictions of the**  
17 **ship-hull, we have developed a parametric model that uses high-level parameters with physical**  
18 **meaning for the generation of ship instances. Thus, the control points of the underlying surface**  
19 **representation are indirectly controlled by these parameters.**

20  
21  
22  
23  
24  
25  
26  
27  
28 The methodology for constructing the parametric ship-hull model is presented in Section 2.  
29 The method is materialized within the Rhinoceros<sup>®</sup>[10] modeling environment, with the aid of its  
30 scripting functionality and Autodesk<sup>®</sup>'s T-Splines<sup>®</sup> Plug-In [11] for Rhinoceros<sup>®</sup>. **It should be**  
31 **noted that the functionality of parametric modeling is not offered by the above software tools; it is**  
32 **in-house developed using the Rhinoscripting programming language.** An early attempt for building  
33 a ship parametric model is due to Lackenby [12] in which hull variants are obtained by modifying  
34 the prismatic coefficient, the center of buoyancy and the extent and position of parallel mid-body  
35 of a parent hull. This method has been subsequently generalized towards improving the geometric  
36 coverage of the parametric model through the use of B-spline techniques; see, e.g., Harries and  
37 Nowacki [13], Kim [14], Abt and Harries [15], Harries [16] and Ping [17]. In previous works of  
38 ours [18, 19], a *Ship Parametric Model (SPM)* has been developed, with the aid of CATIA<sup>®</sup>[20]  
39 modeling environment, resulting in a multi-patch NURBS representation of a ship hull. This  
40 methodology initiated with a list of exposed and internal parameters, which were devised on the  
41 basis of parent hulls and proceeded with the generation of control curve networks, appropriately  
42 augmented with corresponding cross-tangent ribbons. The ship-surface construction was thus  
43 reduced to a sequence of local Hermite interpolation problems which were solved through CATIA  
44 tools, yielding a tangentially-continuous ( $G^1$ ) NURBS multi-patch representation of the ship hull.  
45 In this work, in order to remove deficiencies due to the multi-patch NURBS representation, see [21,  
46 22, 23], we use the T-splines technology, for the construction of the SPM. The methodology initiates  
47 again with a list of exposed and internal parameters, extracted from the form of parent ships. Both  
48 types of parameters are used to parametrically construct the *Control Cage*, which determines the  
49 topology of the unstructured T-mesh and acts as the control “polyhedron” for the generated cubic  
50 T-spline surface. This construction uses Autodesk<sup>®</sup>'s T-Splines<sup>®</sup> Plug-In functionality to produce  
51  
52  
53  
54  
55  
56  
57  
58  
59  
60  
61  
62  
63  
64  
65

1  
2  
3  
4  
5  
6  
7  
8 an analysis suitable T-spline mesh for the ship-hull surface. The produced surface is of higher  
9 smoothness ( $C^2$  continuity) compared to its corresponding NURBS multi-patch representation  
10 ( $G^1$  continuity), except in the vicinity of the extraordinary points, where  $G^1$  continuity is achieved;  
11 see [3].  
12

13  
14 Section 3 is devoted to the presentation of the CFD solver's basic features. The CFD wave  
15 resistance solver is based on the Neumann-Kelvin formulation of the problem, introduced by  
16 Brard [24]; see also [25]. The resulting BIE is numerically solved using a higher order collocated  
17 BEM, which adopts the IGA concept. **The analysis suitable T-Spline representation along with**  
18 **the calculation of collocation points is offered through the IGA export functionality of the T-Spline**  
19 **Plug-In; see [26].** The in-house developed T-spline based IGA-BEM solver is presented in detail  
20 and tested in [21].  
21  
22

23  
24 Section 4 presents the optimization environment integrating the SPM, the T-spline based  
25 IGA-BEM solver and the optimization libraries of modeFrontier<sup>®</sup>[27] for designing ship hulls with  
26 minimum resistance. Finally, two optimization cases (local/global) for a container ship are set-up  
27 and presented in Section 5. The first case deals with bulbous bow optimization (local optimization  
28 problem) against the criterion of minimum wave resistance under a given displacement, while the  
29 second case involves a global ship-hull minimization problem against two objective functions: total  
30 resistance and deviation from a reference ship capacity, i.e., ship's deadweight.  
31  
32

## 33 34 35 36 37 **2. The T-spline Ship Parametric Model (SPM)** 38

39  
40 In this section, we describe a methodology for constructing a parametric model for typical  
41 ship-hull forms constructed within the Rhinoceros<sup>®</sup> modeling environment with the aid of its  
42 scripting functionality and Autodesk<sup>®</sup>'s T-Splines<sup>®</sup> Plug-In for Rhinoceros<sup>®</sup>. Rhinoceros is a  
43 generic NURBS based surface and solid modeler, providing a wide range of functionalities. The  
44 T-Spline plug-in adds T-spline support to Rhinoceros which, with the aid of Rhinoscripting, en-  
45 ables the materialization of the methodology for generating a T-spline ship-hull parametric model.  
46 Finally, the automation offered in Rhinoceros through various scripting languages can easily con-  
47 stitute the developing framework for the creation of the wrapper required in the optimization  
48 process; see §4,5.  
49  
50

51  
52 The basic shape characteristics of a typical ship-hull comprise:  
53

- 54 • a partition of the ship-hull into three main parts, namely the bow, the midship part and the  
55 stern,  
56
- 57 • global dimensions (e.g., length between perpendiculars (Lbp), beam (B), depth (D), draft  
58 (T)) as well as dimensions characterizing each one of the aforementioned ship parts (e.g.,  
59 extent of the midship part),  
60  
61  
62  
63  
64  
65

- a set of control curves that are of boundary (e.g., stern profile, bow profile) or shape-transition character (e.g., FoS (flat-of-side) and FoB (flat-of-bottom) curves) and, finally,
- local geometrical characteristics that serve functional, structural and/or hydrodynamic purposes, e.g., bow-angle of entrance at waterline, bulb-top position, bilge radius, shaft height, etc.

On the basis of the above coarse shape description and a set of parent ship-hulls, a list of *exposed* and *internal* parameters is devised. Exposed parameters will be accessible from the outside of the parametric modeling tool and initiate the modeling process, leading eventually to the production of a corresponding hull instance. On the contrary, internal parameters are not visible from the outside of the parametric tool and are used to control the surface construction process and eventually retain the basic shape characteristics of the parent hulls. Default values for both exposed and internal parameters are extracted from the parent ships. Furthermore, a domain of variation is assigned to each parameter assuring the modeling robustness while at the same time avoiding invalid geometrical models (e.g., self-intersections). These ranges can be thought as confidence intervals and have to be defined through extensive experimentation with the parametric model. Finally, SPM favors the use of non-dimensional parameters where possible, in order to avoid the interdependency between them. Exposed parameters are categorized in four groups, according to whether they are global, associated to the midship, bow and stern areas of the ship. Parameters belonging to the global group correspond to ship’s principal dimensions and their effect is of global nature, e.g.,  $Lwl$ ,  $B$ ,  $T$ ; see Fig. 1. The second category includes parameters that are involved in the generation of the mid-ship part of the ship, e.g.,  $Mid\_L$ ,  $Mid\_Pos$ ; see again Fig. 1. Although not being global in nature, the effect of these parameters is global as the mid-ship part is both the initial and supporting entity in the construction of the hull parametric model. The remaining two categories correspond to the bow and stern parts of the ship and are of more local character as they define shape forms in the areas of the bow and stern, respectively, see Fig. 2. The total number of exposed parameters is 24 and are split as follows: 3 global, 9 for the midship and 7,5 for the bow and stern parts respectively. Both exposed and internal parameters are used to parametrically construct the *Control Cage*, which essentially determines the topology of the T-mesh and acts as the control “polyhedron” for the generated T-spline surface. Specifically, the Control Cage is the T-mesh for a cubic T-Spline, excluding the outer ring of faces that define the boundary conditions.

The Control Cage is uniquely defined by the connectivity and position of its vertices. The connectivity is ship-type dependent and defines the topology. On the other hand, the coordinates of the vertices are parameter dependent and along with the corresponding topology define the final hull-shape. Specifically, if  $\mathbf{X}$  denotes the vector of parameters with  $\mathbf{X} \in \mathbb{R}^m$ ,  $m$  being the total

number of parameters, the T-Spline control points<sup>1</sup>, i.e., the Control Cage vertices  $\mathbf{b}_i$  are defined as  $\mathbf{b}_i(\mathbf{X}) = (b_{ix}(\mathbf{X}), b_{iy}(\mathbf{X}), b_{iz}(\mathbf{X}))$ , where  $b_{ix,y,z}(\mathbf{X})$  are appropriate designer-defined, polynomial functions of the parameter-vector  $\mathbf{X}$ ; see, for example, Fig. 6.

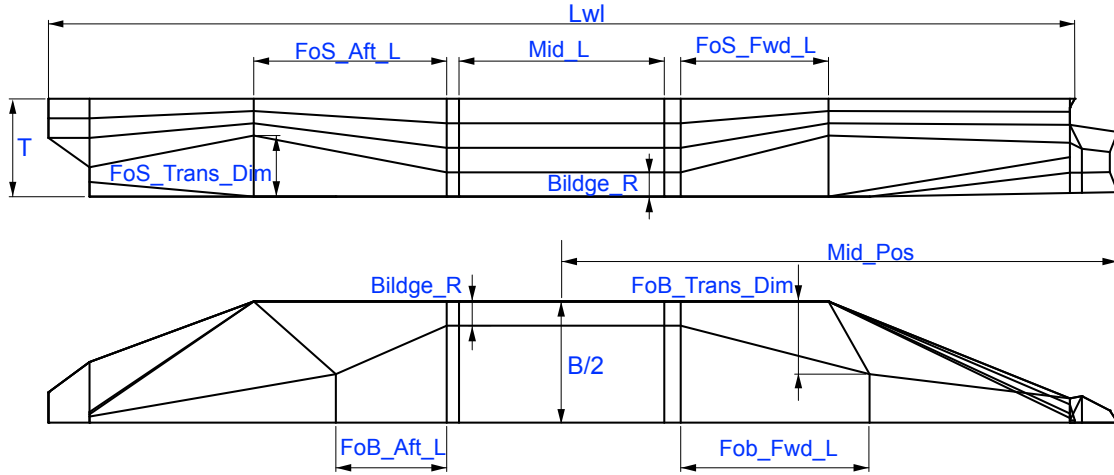


Figure 1: Exposed Global and Midship-part Parameters

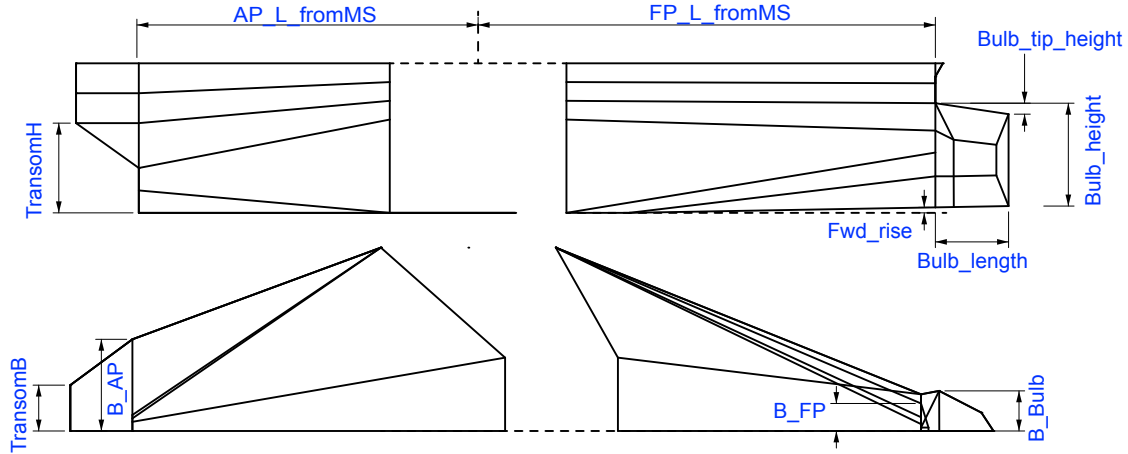


Figure 2: Exposed Bow- and Stern-part Parameters

### SPM Control Cage construction process

Although the whole of the Control Cage is required for the definition of the hull surface, for simplicity's sake, we discuss its construction details in three parts, namely the midship, bow and stern part.

*Mid-ship cage construction:*

For the construction of the mid-ship part, we use six transverse polygonal lines, each comprising six

<sup>1</sup>Excluding the outer ring.

1  
2  
3  
4  
5  
6  
7  
8 line segments. The corresponding vertices of these polygonal lines are connected with longitudinal  
9 connecting lines (red) as shown in Fig. 3. The above polygonal lines define the parallel middle  
10 body and control the fore and aft flat parts of the side and bottom of the ship, namely *Flat of*  
11 *Side* (FoS) and *Flat of Bottom* (FoB). Specifically, the controlling transverse polygonal lines are  
12 the following:  
13  
14

- 15 • **Fwd.Trans** is the boundary of the fore part of the mid-ship and initiates the shape transition  
16 region from mid-ship to bow, while  
17  
18
- 19 • **Aft.Trans** analogously defines the boundary of the aft part of the mid-ship and initiates the  
20 shape transition region from mid-ship to stern.  
21  
22
- 23 • **M1, M2, M3 and M4** correspond to the same L-shaped polygonal line, which is defined by seven  
24 vertices; see Fig. 6 for the case of **M1**. Given that, for a cubic spline, the existence of a  
25 linear segment is guaranteed by the collinearity of four successive control points, the four  
26 L-shaped sections along with the red, orthogonal (w.r.t the sections) connecting lines control  
27 the boundaries of the so-called parallel middle body, i.e., the hull-part with constant section  
28 curves; see again Fig. 3.  
29  
30  
31  
32  
33

34 Both **Fwd.Trans** and **Aft.Trans** have a planar part on the side and bottom of the ship and  
35 thus, along with corresponding segments of **M1, M2, M3, M4**, they guarantee planarity in regions  
36 on the side and bottom of the ship. Specifically, the planarity of 4x4 control points (given the  
37 quadrilateral topology) guarantees the existence of the planar elements in ship's Flat of Side and  
38 Flat of Bottom. For example, the upper parts of **Fwd.Trans, M3, M1** and **M2**, which are coplanar,  
39 generate the forward part of the Flat of Side, while **M1, M2, M4** and **Aft.Trans** generate FoS's aft  
40 part.  
41  
42  
43  
44

45 *Bow- and Stern-part Cage construction:*

46 The bow part (see Fig. 4) comprises the bulb, the upper part of the bow and the transition  
47 from the parallel middle body. **Fwd.Trans** along with the **FP.Crv**, generated at the longitudinal  
48 position of ship's *Fore Perpendicular* (FP), control the shape transition from mid-ship to Bow.  
49 **Bow.Profile** along with **Bulb1,2** polygonal lines define the bulbous bow shape. Once again the  
50 red lines connect the corresponding vertices of the aforementioned polygonal lines.  
51  
52  
53

54 The stern part (see Fig. 5) is mainly defined by the **Aft.Trans, AP.Crv** and **Aft.Profile** polyg-  
55 onal lines. **AP.Crv** is positioned at ship's *After Perpendicular* (AP) and along with **Aft.Trans**  
56 control the shape transition of mid-ship to stern. For the stern shape the transom polygonal line  
57 is also employed.  
58  
59  
60

61 The topological structures in both the stern and bow part are not strictly quadrilateral and  
62 thus, extraordinary points and T-joints are generated.  
63  
64  
65

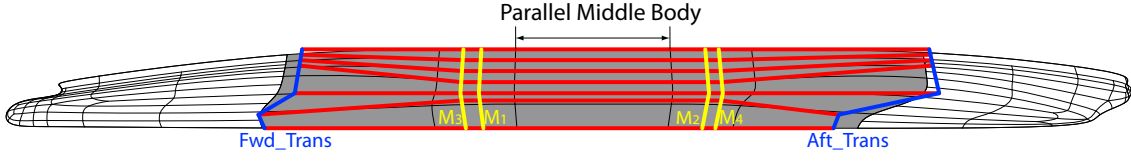


Figure 3: Mid-Ship Cage Construction

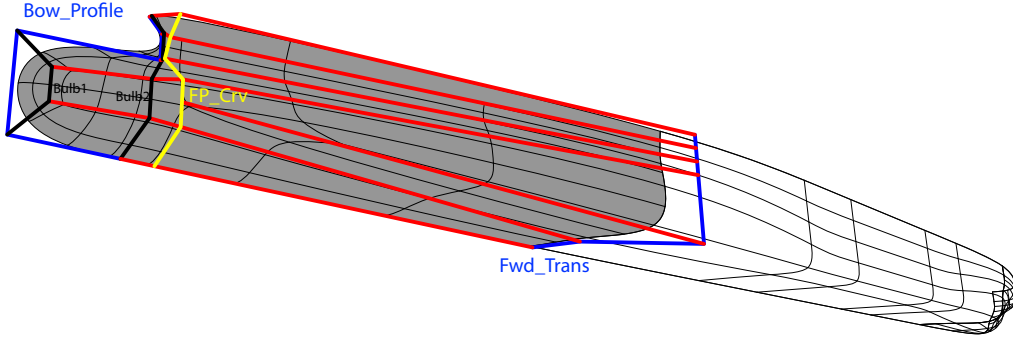


Figure 4: Bow-part Cage Construction

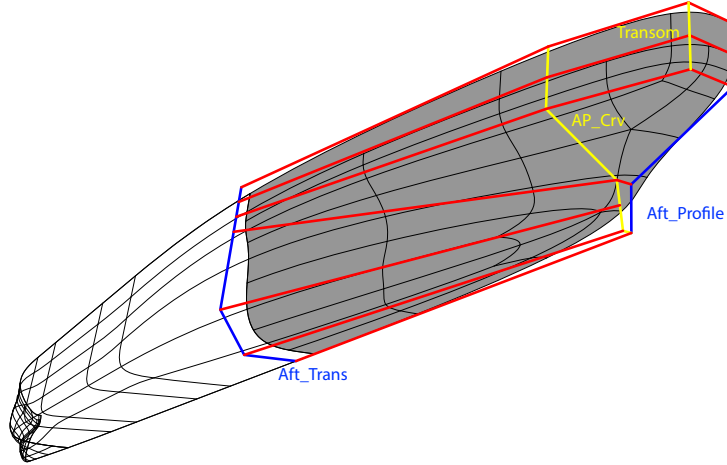


Figure 5: Stern-part Cage Construction

$$\mathbf{b}_0 = \mathbf{O} + \left(-\text{Mid\_pos} + \frac{\text{Mid\_L}}{2}, \frac{B}{2}, 0\right),$$

where  $\mathbf{O}$  denotes the axes origin point.

$$\mathbf{b}_4 = \mathbf{b}_0 + (0, 0, -T)$$

$$\mathbf{b}_3 = \mathbf{b}_4 + (0, 0, \text{Bilge\_R})$$

$$\mathbf{b}_1 = \frac{2}{3}\mathbf{b}_0 + \frac{1}{3}\mathbf{b}_3$$

$$\mathbf{b}_2 = \frac{1}{3}\mathbf{b}_0 + \frac{2}{3}\mathbf{b}_3$$

$$\mathbf{b}_5 = \mathbf{b}_4 + (0, -\text{Bilge\_R}, 0)$$

$$\mathbf{b}_6 = \mathbf{b}_4 + \left(0, -\frac{B}{2}, 0\right)$$

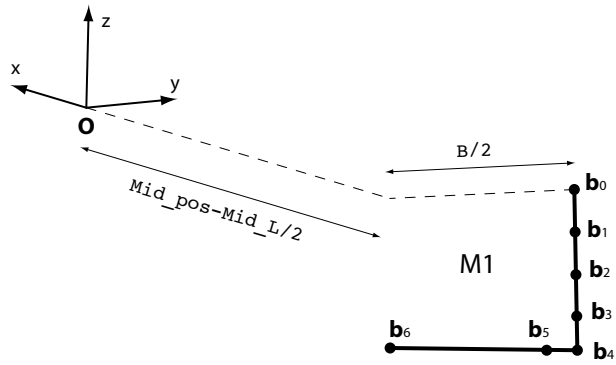


Figure 6: M1 polygonal line



### 3. The IGA-BEM wave resistance solver

For the wave resistance solver, a high-order Boundary Element Method (BEM) based on Iso-Geometric Analysis (IGA) is applied for the numerical solution of the *Boundary Integral Equation* (BIE) (1), as described in detail in [21]. The IGA approach has been initially proposed by Hughes et al [1], in the context of Finite Element Method; see also [28] and [29].

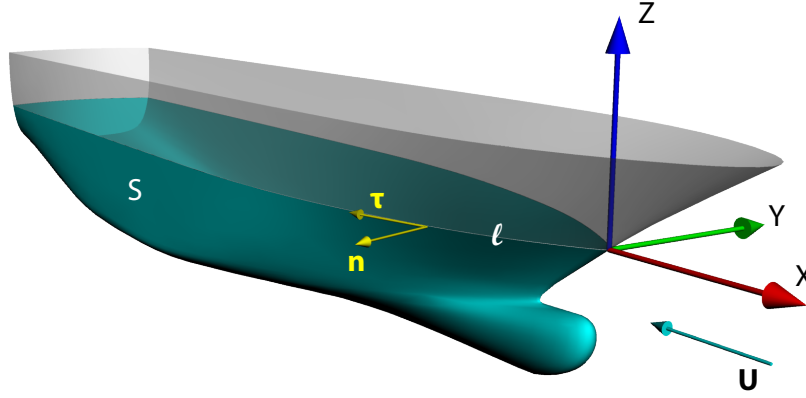


Figure 7: Geometric configuration of the Neumann-Kelvin problem for a surface piercing body.

Following the formulation in Baar & Price [25], the Neumann-Kelvin problem, see Fig. 7, is equivalently formulated as the weakly singular BIE defined on the wetted surface  $S$  and the corresponding waterline  $\ell$ ,

$$\frac{\mu(\mathbf{P})}{2} - \int_S \mu(\mathbf{Q}) \frac{\partial G(\mathbf{P}, \mathbf{Q})}{\partial n(\mathbf{P})} dS(\mathbf{Q}) - \frac{1}{k} \int_{\ell} \mu(\mathbf{Q}) \frac{\partial G^*(\mathbf{P}, \mathbf{Q})}{\partial n(\mathbf{P})} n_x(\mathbf{Q}) \tau_y(\mathbf{Q}) d\ell(\mathbf{Q}) = \mathbf{U} \cdot \mathbf{n}(\mathbf{P}),$$

$$\mathbf{P}, \mathbf{Q} \in S. \quad (1)$$

where  $\mu$  is the density of the Neumann-Kelvin Green function  $G(\mathbf{P}, \mathbf{Q})$ ,  $G^*(\mathbf{P}, \mathbf{Q})$  is Green function's regular part,  $-\mathbf{U}$  denotes the steady forward speed of the ship and  $k = g/\|\mathbf{U}\|^2$  denotes the characteristic wave number, with  $g$  denoting the acceleration due to gravity. From the solution of the above integral equation, various quantities, such as velocity, pressure distribution, ship wave pattern and ship wave resistance can be obtained.

The IGA philosophy attempts to define the approximate field quantities of the boundary-value problem in question from the basis that is being used for representing the geometry of the body boundary. In the case of the boundary integral equation (1), the dependent variable is the source-sink density  $\mu$ , distributed over the body boundary  $S$ . The latter is accurately and efficiently represented as a T-spline surface, see [3, 21], as below:

$$S = \bigcup_{e=1}^{n_e} S_e, \quad S_e(\tilde{\boldsymbol{\xi}}) = \sum_{i=1}^{n_{cp}} \mathbf{b}_i R_i^e(\tilde{\boldsymbol{\xi}}), \quad \tilde{\boldsymbol{\xi}} \in \tilde{\Omega}_e, \quad (2)$$

where  $n_{cp}$  is the number of control points, or T-mesh vertices,  $\mathbf{b}_i$  in the T-mesh,  $\tilde{\Omega}_e$  is the parametric domain of the element  $e$ ,  $R_i^e$  is the restriction of the rational T-spline basis function  $R_i$  at  $\tilde{\Omega}_e$ , and  $n_e$  is the number of elements. In conformity with the IGA concept, the unknown source-sink surface distribution  $\mu$  is approximated by the very same T-splines basis used for the body-boundary representation (2), that is:

$$\mu(\mathbf{P}) = \sum_{i=1}^{n_{cp}} \mu_i \tilde{R}_i(\mathbf{P}), \quad \mathbf{P} \in S, \quad (3)$$

where  $\tilde{R}_i(\mathbf{P}) \equiv R_i^e(\tilde{\boldsymbol{\xi}}(\mathbf{P}))$ ,  $\mathbf{P} \in S_e$ . Inserting Eq. (3) into the BIE (1) we get:

$$\frac{1}{2} \sum_{i=1}^{n_{cp}} \mu_i \tilde{R}_i(\mathbf{P}) - \sum_{i=1}^{n_{cp}} \mu_i \mathbf{n}(\mathbf{P}) \cdot \mathbf{u}_i(\mathbf{P}) = \mathbf{U} \cdot \mathbf{n}(\mathbf{P}), \quad \mathbf{P} \in S, \quad (4)$$

where

$$\begin{aligned} \mathbf{u}_i(\mathbf{P}) = & \int_S \tilde{R}_i(\mathbf{Q}) \nabla_P G(\mathbf{P}, \mathbf{Q}) dS(\mathbf{Q}) + \\ & + k^{-1} \int_\ell \tilde{R}_i(\mathbf{Q}) \nabla_P G^*(\mathbf{P}, \mathbf{Q}) n_1(\mathbf{Q}) \tau_2(\mathbf{Q}) d\ell(\mathbf{Q}) \end{aligned} \quad (5)$$

are the so-called induced velocity factors and  $\nabla_A F(\mathbf{A}, \mathbf{B})$  denotes the gradient of  $F$  with respect to  $\mathbf{A}$ .

We now collocate Eq. (4) by specifying  $n_{cp}$  collocation points  $\mathbf{P}_j, j = 1, \dots, n_{cp}$ , on  $S$ . For smooth ship hulls, these points are chosen to be the 1-ring collocation points for both the non-extraordinary and extraordinary vertices of the T-mesh, as defined in [3]. This definition of collocation points is a generalization of the Greville abscissae for the cases of unstructured grids, T-junctions and extraordinary points. However, when T-splines have no T-junctions or extraordinary points, the 1-ring collocation points described in [3] are equivalent to the two-dimensional Greville abscissae. In this way, we obtain the following linear system of equations with respect to the unknown coefficients  $\mu_i$ :

$$\sum_{i=1}^{n_{cp}} \mu_i \left[ \tilde{R}_i(\mathbf{P}_j) - 2\mathbf{n}(\mathbf{P}_j) \cdot \mathbf{u}_i(\mathbf{P}_j) \right] = 2\mathbf{U} \cdot \mathbf{n}(\mathbf{P}_j), \quad j = 1, \dots, n_{cp}. \quad (6)$$

In the above equation, the integrals involved in the calculation of the induced velocity factors (Eq.5) are localized to integrals over Bézier elements. Moreover, since these singular integrals are defined in the Cauchy Principal Value (CPV) sense, we employ the following technique for their accurate and robust numerical calculation: We exclude an  $\epsilon$ -neighborhood, with  $\epsilon \rightarrow 0$ , around the singularity at the collocation point  $\mathbf{P}_j$  and make sure that the size of integration's intervals, near the singularity, tend to 0 as  $\epsilon \rightarrow 0$ . More details on the treatment of the singular integrals and the achieved rates of convergence can be found in [30]. In order to maintain a uniform numerical scheme for the calculation of the CPV integrals, we need to make sure that the collocation point

1  
2  
3  
4  
5  
6  
7  
8  $\mathbf{P}_j$  lies inside a Bézier element (and not on an edge). If this is not the case, we shift appropriately  
9 the corresponding collocation point.

#### 10 11 **4. The optimization environment**

12  
13  
14 Simulation-based optimization is of growing importance in naval engineering, since it allows to  
15 improve ship performance for a moderate cost, in comparison with costly towing tank experiments.  
16 Moreover, the optimization is conducted in a rigorous algorithmic framework that can outclass  
17 the experience and intuitions of naval architects.

18  
19  
20 A major difficulty to apply an automated shape optimization for complex engineering systems  
21 is the development of a fully automated design loop. Indeed, in our application area, for each  
22 set of parameters, a geometric hull model has to be constructed, allowing the generation of the  
23 computational domain used by the solver to provide the physical response and the performance  
24 analysis. All these steps should be fully automated, without hand-made repairing nor arranging  
25 process, in order to feed the optimization algorithm and finalize the design loop. In this context, the  
26 IGA paradigm offers a significant improvement over the classical grid-based methods, since it relies  
27 on a direct relationship between the design parameters and the solver, without any geometrical  
28 intermediate structures.

29  
30  
31 A second obstacle arises from the simulation process: for complex test-cases, CFD simulations  
32 are expensive, in terms of computational time. Moreover, the numerical solutions obtained can  
33 be polluted by errors arising from the discretization and iterative methods, yielding noisy perfor-  
34 mance evaluations. Sometimes, this may lead the optimizer to spurious local optima or even yield  
35 the failure of the optimization procedure. Here again, the isogeometric context may be helpful  
36 because it allows to avoid geometrical approximations, which reduces the error level, and permits  
37 to construct high-order solutions yielding a better computational efficiency.

38  
39  
40 In summary, isogeometric analysis methods facilitate the development of a design optimization  
41 loop for practical engineering problems and make the resulting tool more efficient. The next section  
42 presents briefly the optimizer considered in the present study and the software environment that  
43 integrates the geometric modeler, the solver and the optimizer.

44  
45  
46 The employed optimizer, as already stated in the introductory section, is modeFrontier<sup>®</sup> from  
47 Esteco. For the first local optimization problem (see §5.1) we utilize the simplex deterministic  
48 algorithm while the second global optimization problem (see §5.2) is handled using the Evolution  
49 Strategy from the evolutionary algorithms offered by the optimizer.

50  
51  
52 A design optimization software environment, depicted schematically in Figure 8, has been set  
53 up including the three main components: the optimizer, the solver and the modeler. Each of these  
54 components is wrapped in a corresponding wrapper, that manages the communication and data  
55 exchange among the components of the optimization environment. The wrappers are implemented  
56  
57  
58  
59  
60  
61  
62  
63  
64  
65

using the python programming language and utilize the TCP/IP network protocol for the required communications. More specifically:

1. Optimizer wrapper (Ow) communicates with the optimizer and broadcasts the generated parameter values to the parametric modeler wrapper (Mw).
2. Mw listens for data connections from Ow. When data, i.e., parameter values, are received, it triggers the Rhino construction script that produces the corresponding instance of the SPM and ultimately stores it in an analysis suitable T-Spline file format (IGA file) at a specified FTP site. If the creation of the IGA file is successful, Ow establishes a connection with the Solver wrapper (Sw) and reports the IGA file creation. If the construction script fails a message is returned to Ow reporting the failure and requesting a new parameter set.
3. When a new IGA file is received, Sw initiates a connection to the site where the IGA file has been saved and retrieves it. IGA BEM solver is then started and performs the resistance calculations resulting, if successful, in the broadcasting of the objective function(s) value(s) to Ow. If computation fails, a network message is returned to Ow reporting the failure and requesting a new parameter set.

As it is obvious from the above discussion Ow, Mw and Sw work at the same time as client and server applications. This constitutes a flexible and efficient software environment for practical tests, presented in the next section.

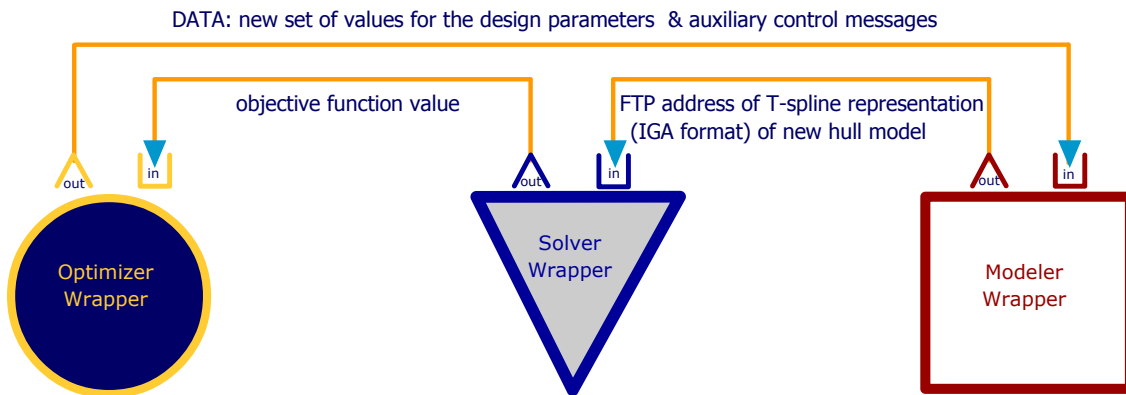


Figure 8: Schematic diagram of the optimization environment

## 5. Container-ship Optimization

The deployment platform for the optimization process is the following:

- The solver component runs in parallel and is deployed on a 8+1 linux cluster (1 head node and 8 working nodes). Each working node is equipped with 2 Quadcore Intel Xeon 2.4GHz CPUs with 12Gb Ram memory.

- Both the optimizer and the solver are deployed on a typical PC
- The intercommunications are carried out over Fast Ethernet connections.

The average time required for each step of the optimization loop is approximately 186 secs. This is split among the processes as follows: On an average, 150 secs are spent in the solving process and 25 secs are used by the modeler. The remaining part is spent by the optimizer and intercommunications.

### 5.1. Constrained bow-optimization for minimizing wave resistance

The optimization environment has been firstly tested for optimizing the bow area of a container ship against the criterion of minimum wave resistance, under the constraint of given displacement  $V = 88581 \text{ m}^3$ . The main particulars of the ship have as follows:  $L_{wl} = 277 \text{ m}$ ,  $B = 32.2 \text{ m}$ ,  $T = 13.0 \text{ m}$ ,  $C_b = 0.734$  and  $V_s=30$  knots. Since we are interested in optimizing the bow ship area, the design parameters are chosen to be: `Bulb_height`, `Bulb_width`, `Bulb_length`, `Fwd_rise`, `Bulb_tip_height` with initial values (0.5, 0.7, 0.7, 0.2, 0.0), respectively ; see Fig. 9. The range of variation of these parameters is given in the table depicted in Figure 9. The bound constraints are handled by modeFrontier while the displacement constraint is fulfilled within the SPM construction process.

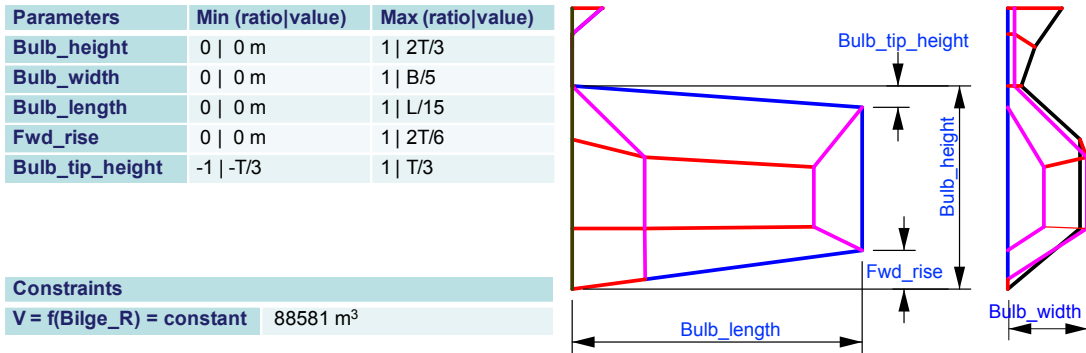


Figure 9: Constrained bow optimization bulb parameters

Figure 10 illustrates the evolution of the wave resistance during the optimization procedure. In this example we attain a 27% reduction in wave resistance, however the initial bulbous-bow shape is not an already optimized one, which justifies the huge attained reduction. Moreover, Figures 11 and 12 depict the bow-area shape for the initial and optimized instance of the parametric model.

As for the example's running time, 446 optimization steps were required for the convergence of the procedure. Thus, given the average time of 186 secs per optimization step, yields a total running time of around 23 hours.

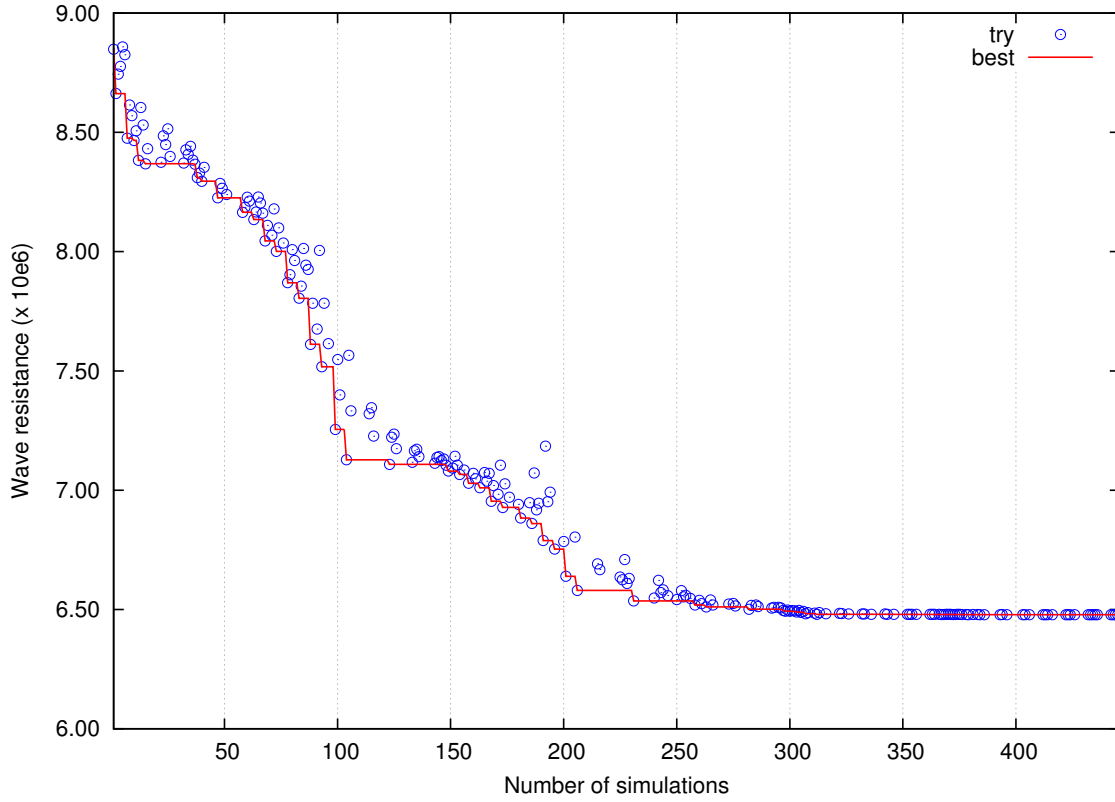


Figure 10: Evolution of wave-resistance for the bulbous bow local optimization

### 5.2. Shape optimization for minimizing resistance and deviation from a target deadweight

As a second test of the optimization environment we globally optimize a ship hull with respect to the following two criteria: a) minimum total resistance  $R_T$  and b) minimum deviation from a reference deadweight of  $DWT=55700$ tons. Total resistance is evaluated using the solver described in §3 as regards its wave component and the standard ITTC relation for the frictional component. The deadweight of the ship is calculated as the difference between its displacement and its lightship, the latter being estimated via empirical formulas for containerships; see, e.g., [31]. The main particulars of the initial ship hull have as follows:  $L_{wl} = 277$  m,  $B = 32.2$  m,  $T = 13.0$  m,  $C_b = 0.734$  while the speed is set to  $V_s=26$  knots.

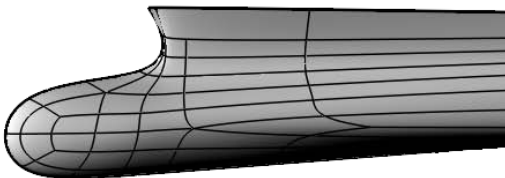


Figure 11: Initial bulbous-bow shape

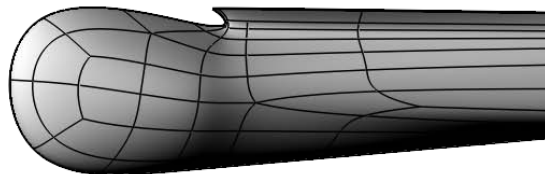


Figure 12: Optimized bulbous-bow shape

Seven design parameters are chosen for the optimization process, namely, the waterline length,  $Lwl$ , the breadth,  $B$ , the longitudinal position of the parallel mid-body,  $Mid\_pos$ , the extent of the parallel mid-body,  $Mid\_L$ , the bilge radius,  $Bilge\_R$ , the bulb length,  $Bulb\_length$  and the bulb width,  $Bulb\_width$ ; see Figures 1,2. The above parameters range as in Table 1. The evolution strategy, offered by modeFrontier, is employed to calculate the Pareto front of the above optimization problem, which is depicted in Figures 15,16, respectively. Figure 15 correspond to a first phase of the optimization process where we try to coarsely cover the feasible space and select a suitable candidate, as an initial point, for the second phase of the optimization process; see Figure 16. In the first phase, the algorithm explores the feasible space with a large step size in order to catch a coarse approximation of the Pareto front, while the second phase refines the step size starting from the previously selected point at the Pareto front. Obviously, the optimum shapes lie on the Pareto front, red line depicted in Figure 16. If, for example, we choose to accept a 150tons deviation from the target deadweight, the optimum solution would be the following ship-hull instance:  $Lwl=295.5m$ ,  $B=32.3m$ ,  $Mid\_pos=0.458$ ,  $Mid\_L=0.1245$ ,  $Bilge\_R=0.0575$ ,  $Bulb\_length=0.973$  and  $Bulb\_width=0.979$  resulting in a resistance value of  $1.915 \times 10^6$  and a deadweight deviation of 139 tons. The shapes of the optimum solution and the initial one is depicted in Figures 14 and 13.

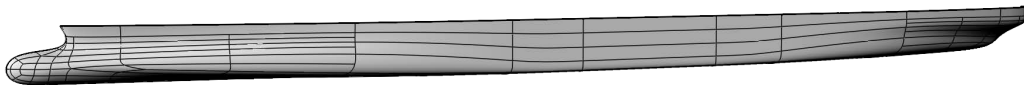


Figure 13: Initial ship

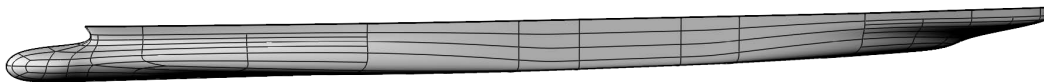


Figure 14: “Optimum” on Pareto front

Table 1: 2nd test of the optimization environment: range of variation of design parameters

$Lwl(m)$	$B(m)$	$Mid\_pos(m)$	$Mid\_L(m)$
$[230,320]$	$[28.9,32.2]$	$[0.45,0.55] \times Lwl$	$[0.1,0.3] \times Lwl$
$Bilge\_R(m)$	$Bulb\_length(m)$		$Bulb\_width(m)$
$[0.05,0.4] \times B/2$	$[0.5,0.99] \times Lwl/15$		$[0.4,0.99] \times B/5$

The required number of steps in this case was around 4000 and thus, given that the optimization step remains same, the total running time climbs to 8.5 days for the same deployment platform.

1  
2  
3  
4  
5  
6  
7  
8  
9  
10  
11  
12  
13  
14  
15  
16  
17  
18  
19  
20  
21  
22  
23  
24  
25  
26  
27  
28  
29  
30  
31  
32  
33  
34  
35  
36  
37  
38  
39  
40  
41  
42  
43  
44  
45  
46  
47  
48  
49  
50  
51  
52  
53  
54  
55  
56  
57  
58  
59  
60  
61  
62  
63  
64  
65

## 6. Conclusion

In this work, we have presented a ship-hull optimization process combining a T-spline based parametric ship-hull model and an Isogeometric Analysis (IGA) hydrodynamic solver for the calculation of ship wave resistance. The parametric modeler is developed within Rhinoceros®[10] modeling environment using Autodesk®'s T-Splines® Plug-In. The surface representation of the generated ship-hull instances comprise one cubic T-spline with extraordinary points, ensuring  $C^2$  continuity everywhere except for the vicinity of extraordinary points where  $G^1$  continuity is achieved. The developed solver is based on the Neumann-Kelvin formulation of the wave-resistance problem, where the resulting Boundary Integral Equation is numerically solved using a higher order collocated Boundary Element Method which adopts the IGA concept and the T-spline representation for the ship-hull surface.

The developed optimization process has been tested in two cases: The first case demonstrates the local optimization of the bulbous-bow area of a container ship, employing 5 relevant parameters, against the criterion of minimum wave resistance, under the constraint of given displacement value. The corresponding running time is around 23 hours for the deployment platform described in §5. The second case involves 7 parameters and 2 objective functions. The parameters used affect the overall hull shape and the minimization objectives include the wave resistance and the deviation from a given deadweight. This time, for the sufficient description of the pareto front, a running time of approximately 8.5 days is required for the same deployment platform.

The two tested cases demonstrate that the developed optimization procedure can be efficiently used for real-life hull-forms solving real-life problems arising in the shipbuilding industry.



1  
2  
3  
4  
5  
6  
7  
8  
9  
10  
11  
12  
13  
14  
15  
16  
17  
18  
19  
20  
21  
22  
23  
24  
25  
26  
27  
28  
29  
30  
31  
32  
33  
34  
35  
36  
37  
38  
39  
40  
41  
42  
43  
44  
45  
46  
47  
48  
49  
50  
51  
52  
53  
54  
55  
56  
57  
58  
59  
60  
61  
62  
63  
64  
65

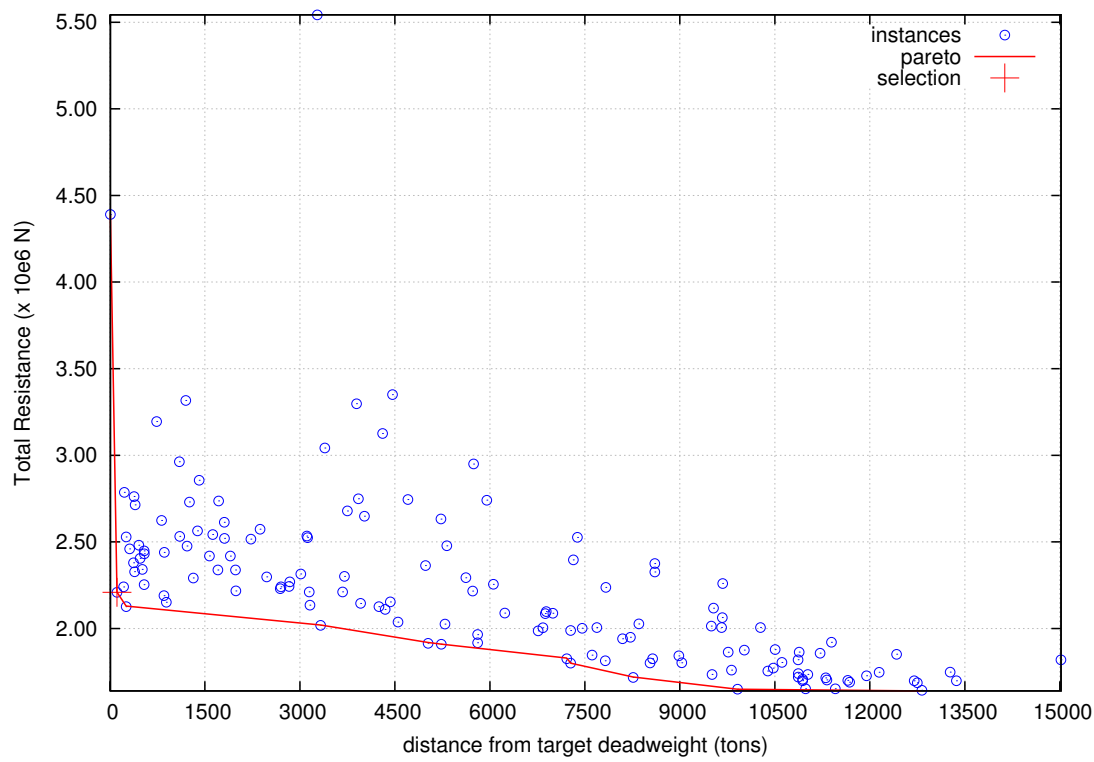


Figure 15: Phase 1: Pareto front for the resistance and the deadweight-deviation criteria

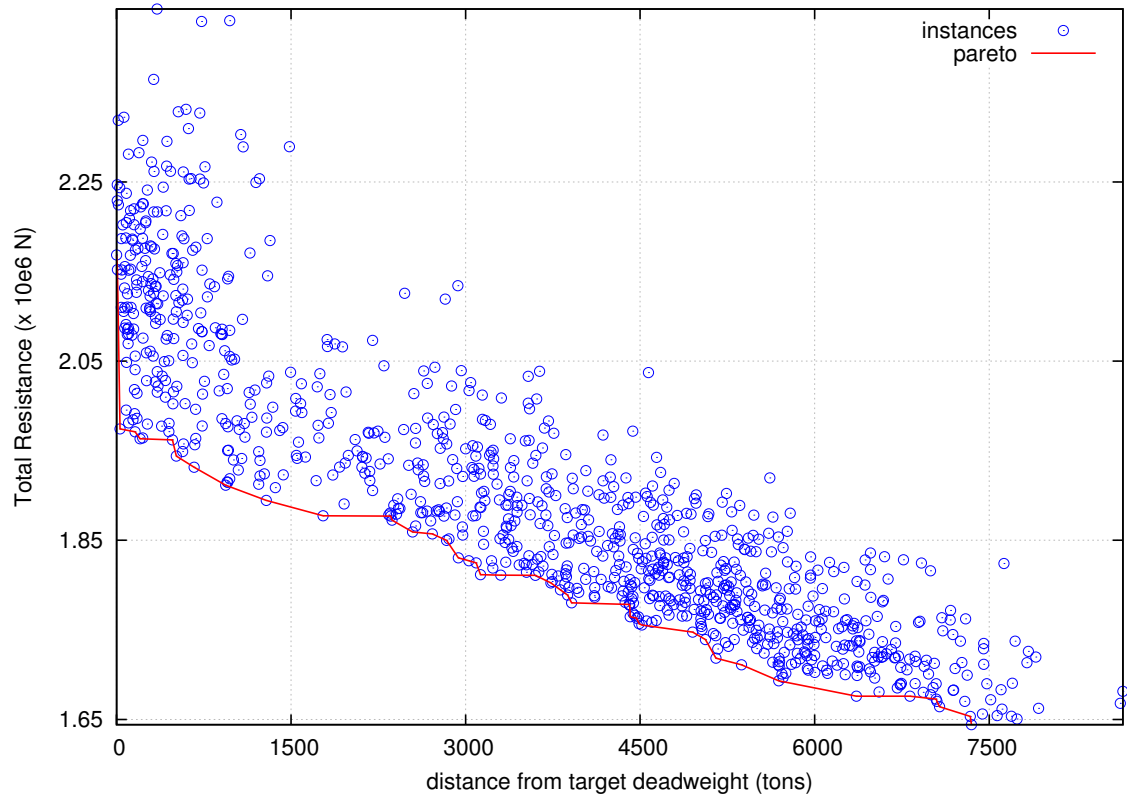


Figure 16: Phase 2: Pareto front for the resistance and the deadweight-deviation criteria

1  
2  
3  
4  
5  
6  
7  
8 **Acknowledgments**  
9

10 This research has been co-financed by the European Union (European Social Fund - ESF) and  
11 Greek national funds through the Operational Program “*Education and Lifelong Learning*” of the  
12 National Strategic Reference Framework (NSRF) - Research Funding Program: THALIS-UOA  
13 (MIS 375891).  
14  
15

16  
17 **References**  
18

- 19  
20 [1] T. J. R. Hughes, J. A. Cottrell, Y. Bazilevs, Isogeometric analysis: CAD, finite elements,  
21 NURBS, exact geometry and mesh refinement, *Computer Methods in Applied Mechanics*  
22 *and Engineering* 194 (2005) 4135–4195.  
23  
24 [2] Y. Bazilevs, V. M. Calo, J. A. Cottrell, J. A. Evans, T. J. R. Hughes, S. Lipton, M. A.  
25 Scott, T. W. Sederberg, Isogeometric analysis using T-splines, *Computer Methods in Applied*  
26 *Mechanics and Engineering* 199 (5-8) (2010) 229–263.  
27  
28 [3] M. A. Scott, R. N. Simpson, J. A. Evans, S. Lipton, S. P. A. Bordas, T. J. R.  
29 Hughes, T. Sederberg, Isogeometric boundary element analysis using unstructured T-splines,  
30 *Computer Methods in Applied Mechanics and Engineering* 254 (0) (2013) 197 – 221.  
31 doi:<http://dx.doi.org/10.1016/j.cma.2012.11.001>.  
32 URL <http://www.sciencedirect.com/science/article/pii/S0045782512003386>  
33  
34 [4] T. W. Sederberg, J. Zheng, A. Bakenov, A. Nasri, T-splines and TNURCCs, *ACM Transac-*  
35 *tions on Graphics* 22 (2003) 477–484.  
36  
37 [5] T. W. Sederberg, D. L. Cardon, G. T. Finnigan, N. S. North, J. Zheng, T. Lyche, T-spline  
38 simplification and local refinement, *ACM Transactions on Graphics* 23 (2004) 276–283.  
39  
40 [6] A. P. Nagy, M. M. Abdalla, Z. Grdal, Isogeometric sizing and shape optimization of beam  
41 structures, in: 50th AIAA/ASME/ASCE/AHS/ASC Structures, Structural Dynamics, and  
42 Materials Conference, Palm Springs, California, USA, 2009.  
43  
44 [7] D. Nguyen, A. Evgrafov, J. Gravesen, Isogeometric shape optimization for electromagnetic  
45 scattering problems, *Progress In Electromagnetics Research* 45 (2012) 117–146.  
46  
47 [8] P. Nørtoft, J. Gravesen, Isogeometric shape optimization in fluid mechanics, *Structural and*  
48 *Multidisciplinary Optimization* 48 (2013) 909–925.  
49  
50 [9] H. Lian, R. Simpson, S. Bordas, Sensitivity analysis and shape optimisation through a t-spline  
51 isogeometric boundary element method, in: *International Conference on Computational Me-*  
52 *chanics (CM13)*, Durham, UK, 2013.  
53  
54  
55  
56  
57  
58  
59  
60  
61  
62  
63  
64  
65

- 1  
2  
3  
4  
5  
6  
7  
8 [10] Robert McNeel & Associates, Rhinoceros, design, model, present, analyze, realize... (2014).  
9 URL <http://www.rhino3d.com/>  
10  
11 [11] Autodesk Inc, T-splines for rhino (2014).  
12 URL <http://www.tsplines.com/>  
13  
14  
15 [12] H. Lackenby, On the Systematic Geometrical Variation of Ship Form, RINA-Transactions 92,  
16 1950.  
17  
18  
19 [13] S. Harries, H. Nowacki, Form Parameter Approach to the Design of Fair Hull Shapes, in:  
20 10th International Conference on Computer Applications (ICCAS), MIT, Cambridge, MA,  
21 USA, 1999.  
22  
23  
24 [14] H. C. Kim, Parametric Design of Ship Hull Forms with a Complex Multiple Domain Surface  
25 Topology, Ph.D. thesis, University of Berlin (2004).  
26  
27  
28 [15] C. Abt, S. Harries, A New Approach to Integration of CAD and CFD for Naval Architects,  
29 in: 6th International Conference on Computer Applications and Information Technology in  
30 Maritime Industries (COMPIT), Cortona, Italy, 2007.  
31  
32  
33  
34 [16] S. Harries, Serious Play in Ship Design, in: Tradition and Future of Ship Design in Berlin.,  
35 Technical University of Berlin, 2008.  
36  
37  
38 [17] P. Zhang, D.-X. Zhu, Parametric Approach to Design of Hull Forms, Journal of Hydrody-  
39 namics 20 (6) (2008) 804-810.  
40  
41  
42 [18] A. I. Ginnis, C. Feurer, K. A. Belibassakis, P. D. Kaklis, K. V. Kostas, T. P. Gerostathis,  
43 C. G. Politis, A catia® ship-parametric model for isogeometric hull optimization with respect  
44 to wave resistance, in: ICCAS 2011, Royal Institution of Naval Architects, 2011.  
45  
46  
47 [19] A. I. Ginnis, R. Duvigneau, C. Politis, K. V. Kostas, K. Belibassakis, T. Gerostathis, P. D.  
48 Kaklis, A Multi-Objective Optimization Environment for Ship-Hull Design based on a BEM-  
49 Isogeometric Solver, in: The fifth Conference on Computational Methods in Marine Engi-  
50 neering (Marine 2013), Hamburg, Germany, on 29-31 May 2013, springer, 2013.  
51  
52  
53  
54 [20] Dassault Systemes, Computer-Aided Three-Dimensional Interactive Application (2014).  
55 URL <http://www.3ds.com/products-services/catia/>  
56  
57  
58 [21] A. I. Ginnis, K. V. Kostas, C. G. Politis, P. D. Kaklis, K. A. Belibassakis, T. P. Gerostathis,  
59 M. A. Scott, T. J. R. Hughes, Isogeometric Boundary-Element Analysis for the Wave-  
60 Resistance Problem using T-splines, Computer Methods in Applied Mechanics and Engi-  
61 neering, submitted 2014.  
62  
63  
64  
65

- 1  
2  
3  
4  
5  
6  
7  
8 [22] R. Sharma, T.-W. Kim, R. Lee Storch, H. J. Hopman, S. O. Erikstad, Challenges in computer  
9 applications for ship and floating structure design and analysis, *CAD 44* (2012) 166–185.  
10  
11 [23] H. J. Koelman, A Mid-Term Outlook on Computer Aided Ship Design, in: *COMPIT’13*  
12 *Proceedings of the 12th International Conference on Computer Applications and Information*  
13 *Technology in the Maritime Industries, Ancona, Italy, 2013*, pp. 110–119.  
14  
15 [24] R. Brard, The representation of a given ship form by singularity distributions when the  
16 boundary condition on the free surface is linearized, *Ship Research 16* (1972) 79–82.  
17  
18 [25] J. J. M. Baar, W. G. Price, Developments in the Calculation of the Wavemaking Resis-  
19 tance of Ships, *Proc. Royal Society of London. Series A, Mathematical and Physical Sciences*  
20 *462* (1850) (1988) 115–147.  
21  
22 [26] M. Scott, T. Hughes, T. Sederberg, M. Sederberg, An integrated approach to engineering  
23 design and analysis using the autodesk t-spline plugin for rhino3d, *Advances in Engineering*  
24 *Software* (in preparation).  
25  
26 [27] Esteco, Integration platform for multi-objective and multi-disciplinary optimization (2014).  
27 URL <http://www.esteco.com/modelfrontier>  
28  
29 [28] J. A. Cottrell, T. J. R. Hughes, A. Reali, Studies of refinement and continuity in isogeometric  
30 structural analysis, *Computer Methods in Applied Mechanics and Engineering 196* (2007)  
31 *4160–4183*.  
32  
33 [29] J. A. Cottrell, T. J. R. Hughes, Y. Bazilevs, *Isogeometric Analysis: Toward Integration of*  
34 *CAD and FEA*, Wiley, 2009.  
35  
36 [30] K. A. Belibassakis, T. P. Gerostathis, K. V. Kostas, C. G. Politis, P. D. Kaklis, A.-A.  
37 Ginnis, C. Feurer, A BEM-Isogeometric method for the ship wave-resistance problem, *Ocean*  
38 *Engineering 60* (2013) 53–67.  
39  
40 [31] Y. Chen, Formulation of a Multi-Disciplinary Design Optimization of Containerships, Mas-  
41 ter’s thesis, Virginia Polytechnic Institute and State University, USA (1999).  
42  
43  
44  
45  
46  
47  
48  
49  
50  
51  
52  
53  
54  
55  
56  
57  
58  
59  
60  
61  
62  
63  
64  
65